



HAL
open science

Effect of finite deformation and deformation rate on partial melting and crystallization in metapelites

Santanu Misra, Jean-Pierre Burg, David Mainprice

► **To cite this version:**

Santanu Misra, Jean-Pierre Burg, David Mainprice. Effect of finite deformation and deformation rate on partial melting and crystallization in metapelites. *Journal of Geophysical Research*, 2011, 116, pp.B02205. 10.1029/2010JB007865 . hal-00617714

HAL Id: hal-00617714

<https://hal.science/hal-00617714>

Submitted on 30 Apr 2021

HAL is a multi-disciplinary open access archive for the deposit and dissemination of scientific research documents, whether they are published or not. The documents may come from teaching and research institutions in France or abroad, or from public or private research centers.

L'archive ouverte pluridisciplinaire **HAL**, est destinée au dépôt et à la diffusion de documents scientifiques de niveau recherche, publiés ou non, émanant des établissements d'enseignement et de recherche français ou étrangers, des laboratoires publics ou privés.

Effect of finite deformation and deformation rate on partial melting and crystallization in metapelites

Santanu Misra,¹ Jean-Pierre Burg,¹ and David Mainprice²

Received 20 July 2010; revised 22 November 2010; accepted 8 December 2010; published 18 February 2011.

[1] Strain and strain rate partitioning in partially molten rocks are two of the important mechanisms that govern the process of coupling and/or decoupling of the partially molten lithosphere. Consequently, the proportion of partial melt and crystals and their network in partially molten rocks influence the degree of the partitioning along with the bulk rheology of the system. This study explores the possible role of finite strain and strain rate on the rate and volume of partial melting and crystallization in a metapelitic system undergoing deformation. Cylinders of synthetic quartz-muscovite aggregate (7:3 volume ratio) were deformed in torsion at 750°C, 300 MPa and constant shear strain rate ($\dot{\gamma} = 3 \times 10^{-4} \text{ s}^{-1}$) for finite shear strains (γ) 1–15. The deformed samples were studied along the longitudinal tangential (LT) and axial (LA) sections to obtain the data along a range of strain rates for a given finite strain and vice versa. The results showed that deformation plays an important role on the kinetics of partial melting and crystallization. With increasing strain rate, amount and rate of crystallization comprise the volumetrically dominant process compared to partial melting at a given finite strain. In contrast, when the strain rate is constant, partial melting is the dominant process over crystallization up to moderate strain ($\gamma < 5$). The dominant process reverses at higher strain, and the system shows more crystallization than partial melting. Application of the experimental data to geological systems implies that for metapelites a significant amount (~20%) of partial melt can generate at high strain rate and moderate strain ($\gamma \sim 7$), but at high strain ($\gamma = 15$) the system is melt depleted. Under such conditions, decoupling should take place in brittle-ductile mode. On the other hand, rocks undergoing deformation with low strain rates and strain ($\gamma < 3$) contain more than 25% partial melt, which can act as a major decoupling agent by localizing ductile shear zones.

Citation: Misra, S., J.-P. Burg, and D. Mainprice (2011), Effect of finite deformation and deformation rate on partial melting and crystallization in metapelites, *J. Geophys. Res.*, 116, B02205, doi:10.1029/2010JB007865.

1. Introduction

[2] Lithospheric-scale decoupling is strongly related to the presence of mechanically weak planar zones, which allow the lithospheric levels to *decouple* from their initial *coupled* architecture. In the ductile crust, the mechanically weak horizons are defined either by compositional gradients [Jordan, 1987] or by the onset, segregation and accumulation of partial melts along a preferred plane [Block and Royden, 1990; Vanderhaeghe and Teyssier, 2001; Vigneresse and Burg, 2004]. Theoretically, lithospheric decoupling has been identified as dependent on several, multiply connected physical and chemical factors, which include various rheological parameters (e.g., flow law, strain rate, finite strain)

of the partially molten rocks [Kirby and Kronenberg, 1987; Barborza and Bergantz, 1998; Vigneresse and Tikoff, 1999; Renner *et al.*, 2000; Burg and Vigneresse, 2002]. Fluid (melt) and solid (crystals) coexist in a partially molten rock. During deformation the solid matrix may undergo brittle fracturing [Dingwell, 1997], plastic deformation [Dell'Angelo and Tullis, 1988] or show granular flow [Misra *et al.*, 2009] depending on the melt content of the system. These different modes of deformation may govern the evolution of crustal decoupling in various ways. Recent nonhydrostatic experimental studies in torsion have demonstrated that shearing plays an important role and can influence the kinetics of partial melting and crystallization compared to hydrostatic conditions where the only deformation mode is isostatic compaction, given the other intrinsic and extrinsic parameters constant [Misra *et al.*, 2009]. Axial compression experiments conducted by Holyoke and Rushmer [2002] showed that there is a difference in the amount of melt generation, hence melt pore pressure buildup, between muscovite and biotite dehydration melt-

¹Structural Geology and Tectonics Group, Geological Institute, ETH, Zurich, Switzerland.

²Géosciences Montpellier UMR CNRS 5243, Université Montpellier 2, Montpellier, France.

Table 1. List of Experiments Described in This Paper With Relevant Data and Comments^a

Experiment	CP	T	$\dot{\gamma}_{\max}$	γ_{\max}	Plane of Observation	
1	P1013	300	750	3×10^{-4}	1.0	LT section
2	P1026	300	750	3×10^{-4}	2.5	LT section
3	P1005	300	750	3×10^{-4}	3.0	LT section
4	P1146	300	750	3×10^{-4}	5.0	LT and LA section
5	P1025	300	750	3×10^{-4}	7.0	LT section
6	P1161	300	750	3×10^{-4}	10.0	LT and LA section
7	P1095	300	750	3×10^{-4}	15.0	LT and LA section

^aSee text for details. CP, confining pressure (in MPa); T, temperature (in °C); $\dot{\gamma}_{\max}$, shear strain rate at the outer boundary of the cylindrical sample (in s^{-1}); and γ_{\max} , finite shear strain at the outer boundary of the cylindrical sample.

ing, thereby affecting melt-induced microstructures and melt connectivity. Partial melt generated during muscovite dehydration melting localizes along permeable cataclastic zones produced during deformation, whereas melt from biotite dehydration melting accumulates along grain boundaries. These two contrasting segregation sites (i.e., either by fracturing or grain boundary wetting) control the generation of melt fraction in these two systems. This study indicates that the composition of the parent rock also influences the rate and amount of partial melting along with other physical and chemical factors. However, in natural settings, the proportion of fluid phases with respect to the solid phase continuously changes during melting and crystallization of the rock, which results in a significant change of both material and stress transport properties [Laporte and Watson, 1995]. In addition, the amount of fluid phase (melt) controls the magnitude of strain and strain rate partitioning between the fluid and the solid phase. Burg and Vigneresse [2002] studied theoretically the interactions between melting, melt segregation, crystallization and crystal interactions with deformation and concluded that solid-to-suspension transitions during melting and crystallization in a dynamic setting are not symmetrical. They further established that the cycle of melting and crystallization and their mutual interactions are related nonlinearly with time and space resulting in feedback loops, some of which are positive and the others negative during melting and crystallization, respectively. The study of strain rate dependence on melting and crystallization is thus important for the mechanics of melt-rock systems, where partial melting or crystallization accompany deformation. It is also important to take into account the effects of progressive deformation, which governs the evolution of deformation-induced microstructures, formation of partial melt and new crystals.

[3] A systematic study of the generation of partial melt and crystallization as functions of strain and strain rate is lacking in the geological literature. Experimental investigations were mostly conducted to explore the rheology of partially molten rocks where the starting materials, in most of the studies, are considered to have a constant amount of glass, melt or analog of melt [Zimmerman et al., 1999; Rosenberg and Handy, 2000; Holtzman et al., 2003]. Deformation experiments of rock samples with granitic composition have been performed at high pressure and temperature to study how the amount and distribution of melt fraction influences the bulk rheology [van der Molen and Paterson, 1979; Rutter and Neumann, 1995; Rushmer, 1995]. In these experimental investigations, the

authors increased the melt fractions either by varying the amount of water at constant temperature [van der Molen and Paterson, 1979] or by increasing temperature [Rutter and Neumann, 1995]. However, crystallization under isothermal shearing is much discussed in other sciences, particularly in polymer material engineering. Several investigations demonstrated that the rate of shearing and shear strain greatly influence this process by [Lagasse and Maxwell, 1976; Keller and Kolnaar, 1998; Janeschitz-Kriegl et al., 2003; Zheng and Kennedy, 2004; Tanner and Qi, 2005]. They also revealed a fair agreement between experiments and theory and concluded that a simple strain and strain rate function can provide a reasonable description of deformation-induced crystallization.

[4] In this paper, the strain and strain rate dependence of partial melting and crystallization has been investigated experimentally and the results are discussed in terms of possible geological applications. As starting materials we used fine grained, synthetic quartz muscovite samples of constant chemical compositions and physical properties. The samples were deformed in torsion at elevated pressure and temperature. The deformed samples were observed and analyzed in two principal sections to get comparable data for different strains and strain rates.

2. Experimental Methods and Analyses

[5] Deformation experiments were performed on very fine grained synthetic aggregates of muscovite and quartz received from A. Luisoni (<http://www.a-luisoni.ch>). The grain sizes of quartz and muscovite were 4–6 and 30–40 μm , respectively. Muscovite has a chemical composition of $(\text{K}_{0.9}\text{Na}_{0.1})(\text{Al}_{1.6}\text{Fe}_{0.3}\text{Mg}_{0.1})[\text{Si}_{3.2}\text{Al}_{0.8}\text{O}_{10}](\text{OH})_2$. Muscovite and quartz powder were mixed homogeneously in 30% and 70% by volume, respectively. The synthetic rock was fabricated by first uniaxial pressing of the mixed dry powder at 200 MPa, at room temperature, and in a steel canister. The canister was closed by welding and then was hot pressed isostatically (HIP) at 160 MPa and 580°C for 24 h. The values of hydrostatic pressure and temperature for HIP were chosen to avoid any reaction and/or melting between the starting compositions [Brearley and Rubie, 1990]. After hot pressing, the solid material showed that quartz and muscovite had not reacted during preparation and retained their original composition. The starting material had porosity between 12 and 15% and a strong foliation defined by muscovite grains. Cylindrical samples of 10 mm diameter were cored with the HIP-derived foliation perpendicular to the cylinder axis. The samples were deformed in torsion in an internally heated gas-medium apparatus [Paterson and Olgaard, 2000] at 300 MPa confining pressure and 750°C temperature with constant shear strain rate ($\dot{\gamma} = 3 \times 10^{-4} \text{ s}^{-1}$) to achieve maximum shear strains ranging from 1.0 to 15.0.

[6] All deformed samples (Table 1) were observed along longitudinal tangential (LT) sections and three of them along longitudinal axial (LA) sections (Figure 1), which are the two principal planes of observation for torsion experiments [Paterson and Olgaard, 2000]. The bulk shear direction is orthogonal and parallel to the LA and LT sections, respectively. In addition, LA planes contain the axis of rotation, where the deformation is zero at the axis of rotation and increases with radial distance in the lateral

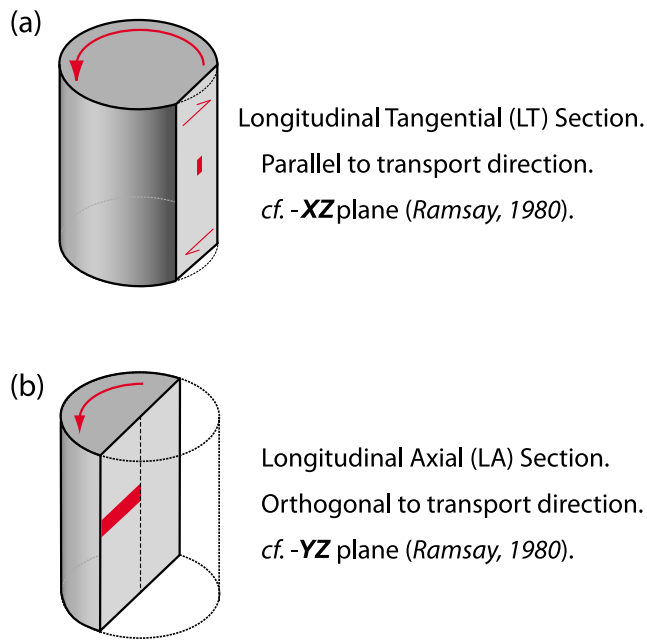
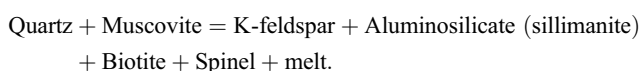


Figure 1. Schematic illustrations showing the two principal planes of observations of deformed samples: (a) longitudinal tangential section and (b) longitudinal axial section. In Figure 1a the red square shows the location of imaging, whereas in Figure 1b a series of images were taken along the red strip. The illustrations are not to scale.

direction; both the rate and amount of shear strain increase linearly (independent of rheology). This unique feature of this plane allows measurement of the area fractions of partial melt and crystallization at different positions with the same amount of finite shear strain but varying shear strain rate and vice versa.

3. Results

[7] While achieving the experimental conditions, the samples showed hydrostatic compaction as the target confining pressure (300 MPa) and temperature (750°C) of the deformation experiments were higher than those of the hot press conditions (160 MPa and 580°C). The porosity of the starting samples (12–15%), in general, decreased because of compaction and showed ~5% porosity at 300 MPa and 750°C. The porosity further reduced after the introduction of deformation (1 to 2% porosity at $\gamma = 1.5$). With progressive deformation, melt was generated while new minerals, mostly K-feldspar, biotite, sillimanite and accessory spinel, crystallized [Misra *et al.*, 2009]. The chemical reaction can be generalized as



Area fractions of partial melt and new crystals were measured in images recorded in the backscattered electron (BSE) mode of a scanning electron microscope (SEM). Images of interest were transformed to a binary image with

a suitable tolerance value for the corresponding phases and the area percentage was measured with the ImageJ open source software (<http://rsbweb.nih.gov/ij/index.html>). A single datum in the plot represents the average value of 5 to 7 measurements normalized by assuming that the sum of all phases is 100%. It was not possible to measure separately biotite and spinel, as they have very similar gray levels in BSE images. In the following descriptions and discussions, we refer to them together as “biotites.” The finite shear strain (γ) varies from zero at the center to a maximum value at the outer radius end. The values measured on the outer radius end of the tangential section (LT) and the finite strains measured at smaller radii inside (on LA section) the deformed samples will be referred as γ_{\max} and γ_{in} , respectively. The same convention will be followed for shear strain rate (i.e., $\dot{\gamma}_{\max}$ and $\dot{\gamma}_{\text{in}}$).

[8] Figures 2a–2d show representative BSE images of four of the seven deformed samples (at $\gamma_{\max} = 1, 7, 10$ and 15). The initial shear plane parallel planar fabric defined by flaky muscovite grains showed back rotation in response to the shear deformation and their long axes aligned crudely along the maximum stretching direction (Figure 2a). The quartz grains behaved as rigid objects. The initial sharp grain boundaries were smoothed during partial melting. The distributions of melt, K-feldspar and biotites, as an example, are shown separately from the microphotograph 2 (Figure 2c) in Figures 2e–2g, respectively. The area measurements (in %) of partial melt and newly formed crystals in deformed samples as a function of finite shear strain ($\gamma_{\max} = 0$ –15) are shown in Figure 2h. The measurements were performed along LT sections of each of the seven deformed samples, which were deformed at constant strain rate ($\dot{\gamma}_{\max} = 3 \times 10^{-4} \text{ s}^{-1}$), confining pressure (300 MPa) and temperature (750°C). Comparison of the amount of melt and new crystals shows that in the beginning (up to $\gamma_{\max} = 3$) melting is dominating (~12–15%) over crystallization of a small amount (~2–3%) of biotites. However, rate and amount of K-feldspar crystallization increased rapidly after $\gamma_{\max} = 3$, and the K-feldspar amount reached ~22% at $\gamma_{\max} = 5$, whereas the amounts of partial melt and biotites were 14% and 5%, respectively. Partial melting reached its highest value (~21%) at $\gamma_{\max} = 7$ and this amount steadily decreased to zero with further deformation (up to $\gamma_{\max} = 15$). The amount of K-feldspar, on the other hand, continuously increased up to 33% at $\gamma_{\max} = 15$. The amount of biotites was nearly constant within a range of 3–5% from $\gamma_{\max} = 5$ to 15. The amount of the two starting materials (70% quartz and 30% muscovite) decreased with progressive deformation, which confirms that melt and new crystals were formed at the expense of the starting mineral phases. All muscovite grains were broken and gradually consumed by the dehydration reaction. They were totally consumed after $\gamma_{\max} = 10$. The contribution of quartz to the reaction products was about 20% and the system contained 50% of quartz at the end of the series ($\gamma_{\max} = 15$).

[9] Three samples, which were deformed to a maximum finite shear strain (γ_{\max}) 5, 10 and 15 (experiments P1146, P1161 and P1095, see Table 1) at their outer boundaries, were cut along their LA planes to observe the amount of melt and new crystals as a function of shear strain rate ($\dot{\gamma}$). Panoramic views of the three samples from their center to

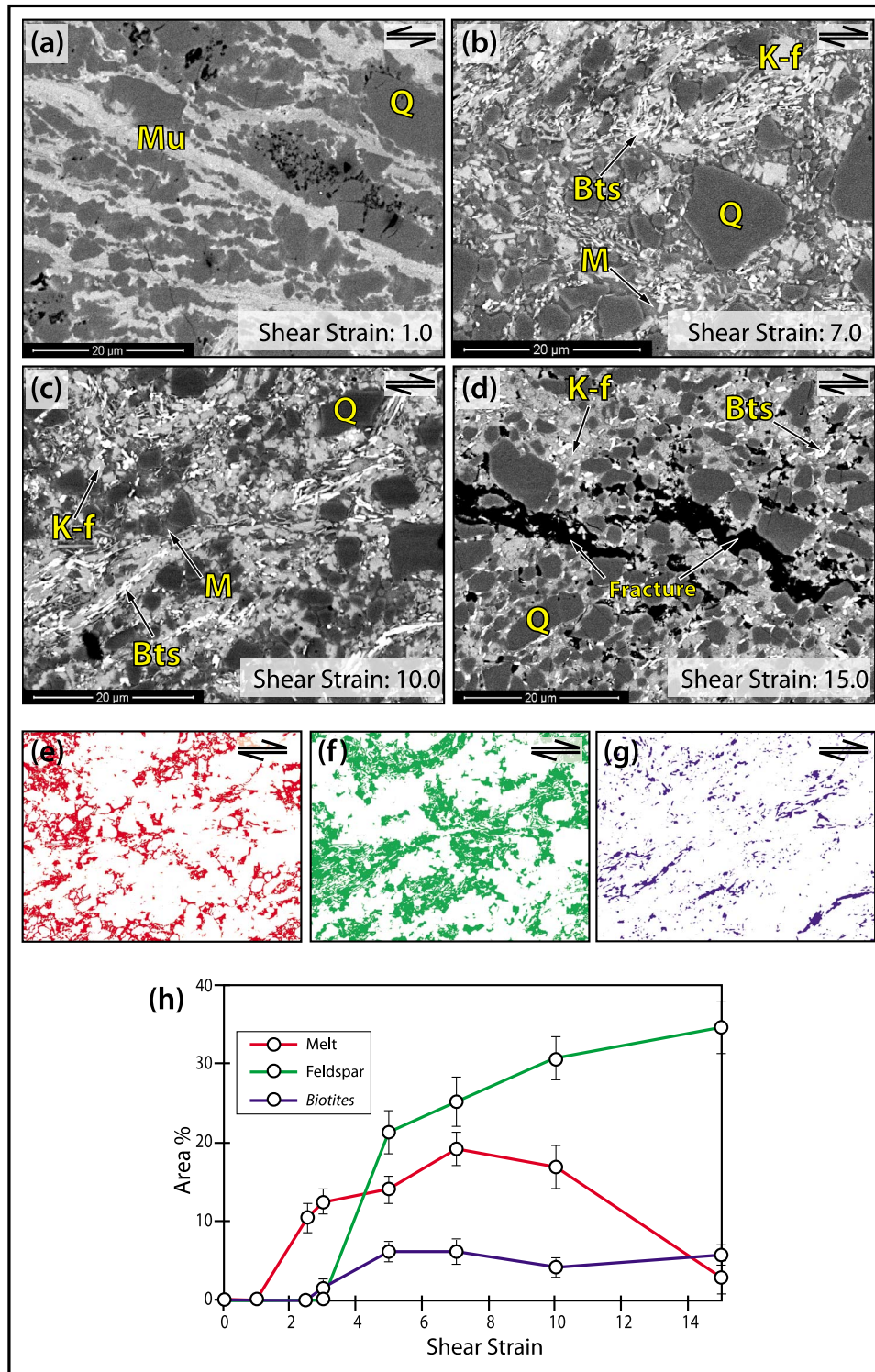


Figure 2. (a–d) Microphotographs showing distribution of starting aggregates and the reaction products (Q, quartz; Mu, muscovite; M, partial melt; K-f, K-feldspar; and Bts, biotites). The two diagonal black shapes in Figure 2d are fractures, developed during torsion experiments at $\gamma_{\max} = 15$. Distribution of (e) partial melt, (f) K-feldspar, and (g) biotites in a deformed sample ($\gamma = 10$), measured on Figure 2c. (h) Variation of the amount (area %) of partial melt, K-feldspar, and biotites with progressive finite shear strain.

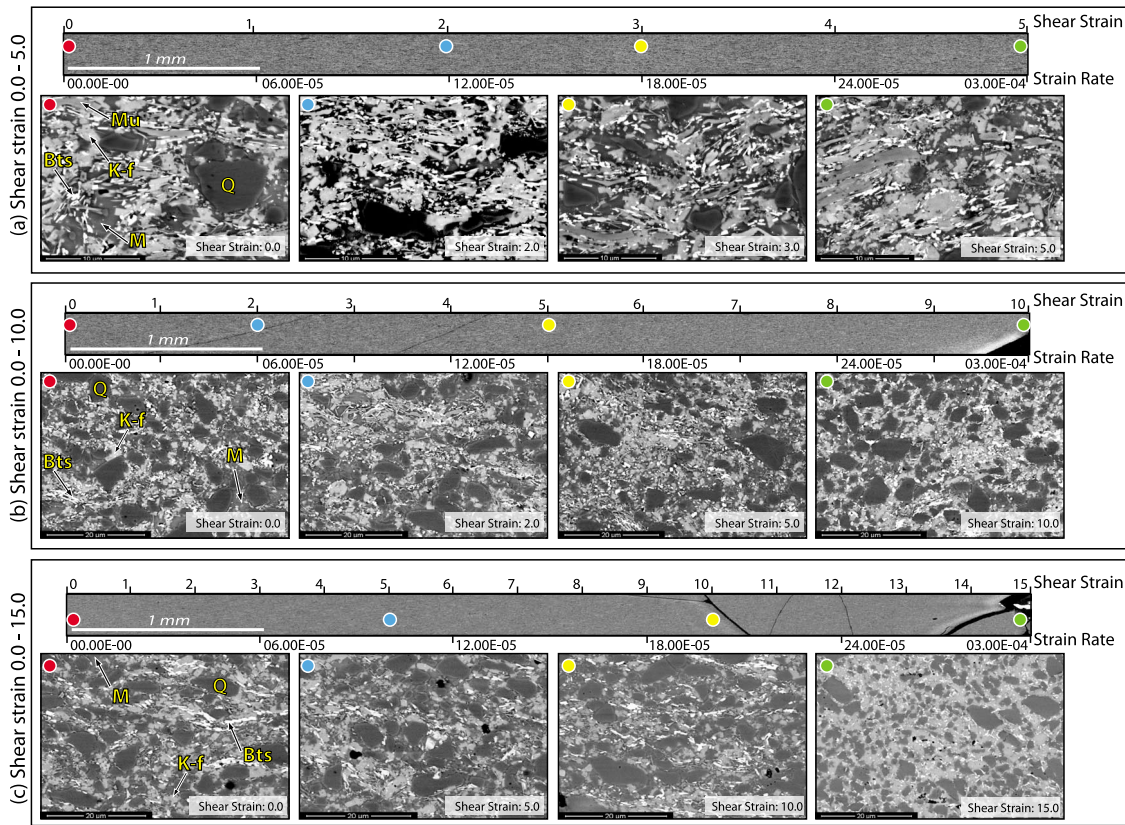


Figure 3. Observation of phase distribution of three deformed samples cut along the longitudinal axial section (see Table 1). The three long strips show the view of the LA sections from the center (left, where strain and strain rate are zero) of the sample to the outer edge (right, where strain and strain rate are maximum). Considering the linear dependence of strain rate and strain with the radius of the samples, the strips were scaled for shear strain and strain rate. For each of the three samples, four representative microphotographs are shown for different strain rate and strain. Q, quartz; Mu, muscovite; M, partial melt; K-f, K-feldspar; and Bts, biotites.

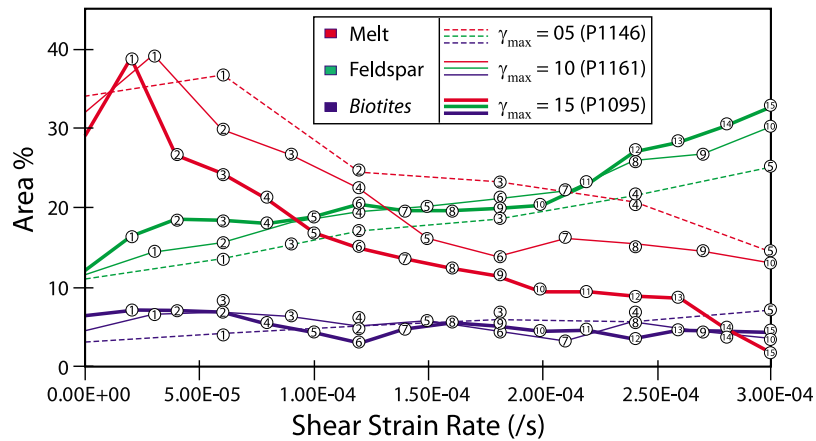


Figure 4. Plot of shear strain versus area (%) showing the generation of partial melt (red curves) and crystallization (green curves and violet curves represent corresponding amounts of K-feldspar and biotites, respectively) for three different samples deformed at $\gamma_{max} = 5$ (dashed lines), 10 (thin lines), and 15 (thick lines). Measurements were performed along the longitudinal axial sections as shown in Figure 3. The digits inside the circles on the curves indicate the amount of finite shear strain on that point.

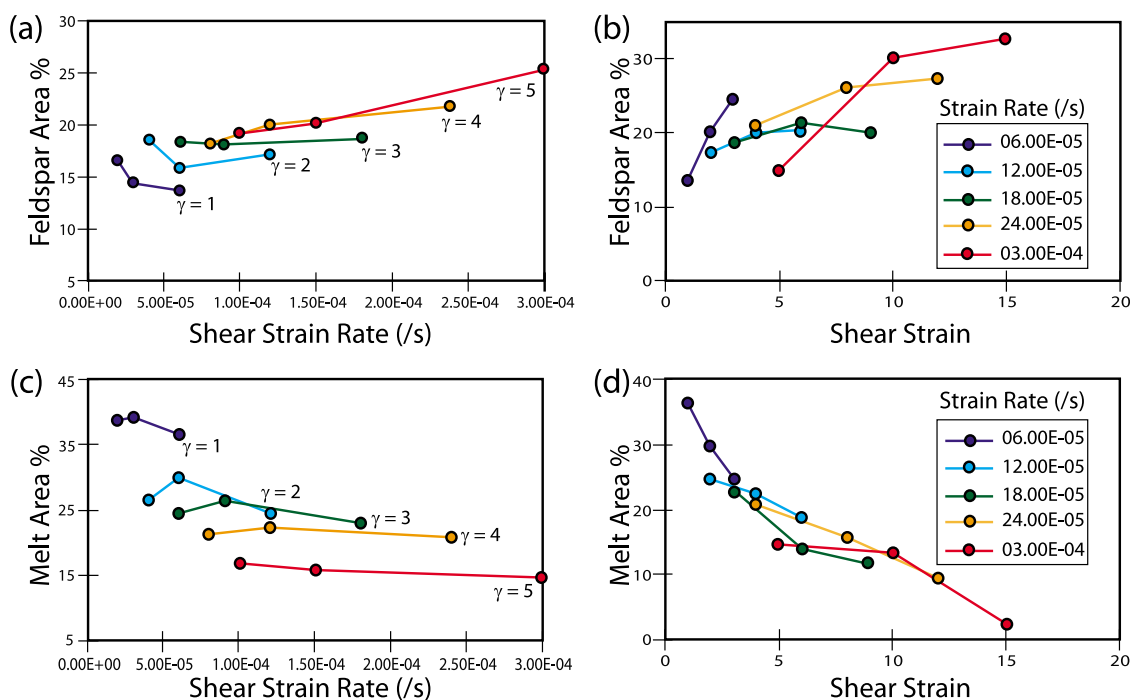


Figure 5. Measured data of the amount of partial melting and crystallization described in area (%) versus strain rate–strain plots. (a and b) Amount of K-feldspar for given constant strains with varying strain rate and vice versa, respectively. (c and d) Same as Figures 5a and 5b except for amount of partial melt.

outer edge as observed in SEM are shown in Figure 3. The sections are marked with scales of finite strain and strain rate at their top and bottom, respectively. From each section, four representative BSE images were presented to show the characteristic microstructures and melt–crystal distribution as functions of finite strain and strain rate.

[10] Variation of the amount of melt, K-feldspar and biotites with respect to measured shear strain rate along the radius of the deformed samples are presented in Figure 4. The data obtained from the center of the samples, where finite strain and strain rate are zero, can be considered for hydrostatic experiments at 750°C and 300 MPa. The plot reveals that the relative amount of biotites remains almost constant (~5%) and independent of shear strain rate and finite deformation. However, the trend of melt and new crystals of K-feldspar contents shows a strong dependence upon strain rate. In general, irrespective of the finite shear strain, crystallization of K-feldspar increases with strain rate whereas the amount of partial melt decreases with strain rate.

[11] With the help of the experimental data presented in Figure 4, it is possible to plot the amount of melt and new crystals as a function of finite shear strain when strain rate is constant and vice versa. We took the amount of K-feldspar to represent crystallization since the amount of biotites is constant. The measurements are shown in four separate diagrams in Figure 5. Crystallization of K-feldspar shows a complex behavior at low strain, but increases with strain rate at high strain ($\gamma_{in} = 4\text{--}5$; Figure 5a). The fraction of K-feldspar increases with increasing shear strain for a given strain rate. For example, at constant $\dot{\gamma}_{in} = 6 \times 10^{-5} \text{ s}^{-1}$, the number of K-feldspar crystals augments by about 12% when finite shear strain (γ_{in}) is increased from 1 to 3.

(Figure 5b). The amount of melt does not change with increasing shear strain rate for a given finite strain, particularly at higher strain ($\gamma_{in} = 5$; Figure 5c), but decreases almost linearly with progressive shear strain for a given strain rate (Figure 5d).

4. Discussion

[12] The experimental results reveal that both finite strain and strain rate play critical roles on the rate and amount of melt production and the creation of neoblasts under dynamic shear flow. The experiments were conducted at isothermal and isobaric conditions to minimize the potential effects of temperature and pressure. The evolution of the whole system starting from solid, quartz-muscovite aggregates to a two-phase solid–fluid system (quartz, muscovite, K-feldspar, biotites crystals–partial melt) has also rheological consequences [Vigneresse *et al.*, 1996; Misra *et al.*, 2009]. However, we will mainly focus on the critical role of strain and strain rate on partial melting and crystallization with possible geological implications. The bulk response of partially molten rocks to tectonic stresses at different strain rates has been discussed theoretically by Vigneresse and Burg [2004], and their results are considered and compared here with an additional parameter – finite strain, together with the strain rate.

[13] Our experimental data showed that, with increasing strain ($\gamma_{max} > 4$), crystallization of new minerals dominates partial melting for a given finite strain rate ($\dot{\gamma}_{max} = 3 \times 10^{-4} \text{ s}^{-1}$; Figure 2h). With progressive shearing at the same strain rate the behavior of melt production is complex. The amount of melt increases almost linearly up to $\gamma_{max} = 7$,

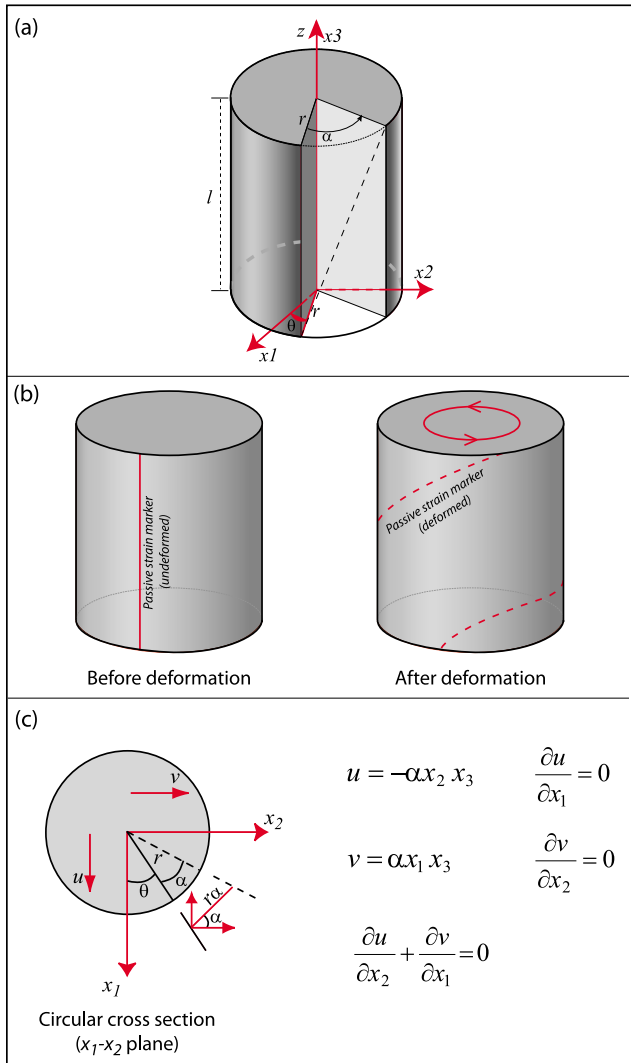


Figure 6. Schematic diagrams to describe the three basic assumptions adopted in this study. (a) Shear strain and strain rate increases linearly from the center to the outer edge of the sample for a constant angular displacement rate (see text for details). (b) The deformation is homogeneous and does not involve any volume change. (c) The velocity gradients ($\partial u/\partial x_1$ and $\partial v/\partial x_2$) acting on the cross section of the cylinder, cut perpendicular to the rotation axis, are zero, allowing no movement of partial melt and crystals along the radius on the plane.

then decreases to zero following approximately the same, but negative slope from $\gamma_{\max} = 7-15$. However, it is impossible to dissociate strain from kinetic effects in experiments where strain varies linearly with time. The kinetic effects associated with diffusion length (x) are related to time (t) by its square root ($x \approx \sqrt{Dt}$, where D is the diffusivity of the system under consideration; [e.g., Brady, 1995; Béjina et al., 2003; Watson and Baxter, 2007]). The amount of melt and new crystals as functions of progressive deformation (Figure 2h) did not reach a stable value. We take this observation as evidence that the syndeformation melting and crystallization reactions did

not achieve chemical equilibrium under dynamic conditions. The reaction products, new crystals and melt-rich pockets are too tiny to quantify and judge whether they had equilibrium chemical composition. This technical problem also does not allow balancing chemically the reactants (quartz and muscovite) and the reaction products (K-feldspar, biotites, melt, etc.). The data presented are thus instantaneous, corresponding to local finite strain and strain rate. In summary, at high strain rate and finite strain, the rate and amount of new crystals increases and the system becomes melt-depleted. Under such conditions, fracturing is expected [Dingwell, 1997]. This is also revealed in our experiment. At $\gamma = 15$, the sample showed brittle fracturing in response to deformation (Figure 2h). The fracture patterns include both Mode I (opening) and Mode II (low angle Riedel shear fracture). Prior to fracturing, the original crystals of the aggregate may undergo plastic deformation and may exhibit a preferred crystalline orientation. The new crystals growing under dynamic conditions may also show both shape and crystallographic preferred orientations. However, this hypothesis needs to be proven by systematic experimental investigation. The decoupling zones would favor increase in strain rate, which would tend to enhance crystallization and therefore harden the system. The decoupling mechanism would be in the so-called brittle-ductile transition domain, which may locally involve very high strain rate resulting in earthquake slip rates.

[14] At low strain rates and finite strain, melt generation dominates over new crystallization. The rock would contain a significant amount of melt ($\sim 30\%$), which can segregate and accumulate as pockets or veins, giving rise to migmatitic rocks as described in classical text books [e.g., Mehnert, 1968; Ashworth, 1985]. Under deformation these mechanically weak pockets and channels form heterogeneous rock domains crucial for localizing deformation in decoupling zones at low strain rate [e.g., Vanderhaeghe et al., 1999; Brown, 2001; Hamilton, 2007].

[15] Our experiments are based on three assumptions: (1) the strain rate and finite strain increase linearly from center to the outer boundary of the sample for a given constant displacement rate [Paterson and Olgaard, 2000], (2) the deformation of the samples is homogeneous at the macroscopic scale and the sample geometry does not change with progressive torsion, and (3) the melt and solid crystals do not migrate along the radius on the plane orthogonal to the cylindrical sample axis [King et al., 2010]. The classical equations that relate strain rate ($\dot{\gamma}$) and shear strain (γ) with the sample geometry for a given angular displacement (α) and angular displacement rate ($\dot{\alpha}$) are $\gamma = r\alpha/l$ and $\dot{\gamma} = r\dot{\alpha}/l$, where r and l are any given radius measured from the center of the circular cross section of the sample and length of the cylinder, respectively (Figure 6a). These two equations describe the linear dependence of strain and strain rate with the radius during torsion experiment, which is independent of the material rheology, i.e., this is solely a finite strain effect. The second assumption is not absolutely true for our experiments, particularly at the beginning of deformation ($\gamma = 0$ to 1.5), because of compaction strain (porosity reduction $\sim 3\%$). However, we applied the generalization of constant geometry to samples deformed at high strain ($\gamma_{\max} > 5$) to simplify our analysis (Figure 6b). For the

third consideration, it needs to be proven that there is no mean stress gradient on the plane of measurement (i.e., the longitudinal axial plane). Several workers, particularly in material sciences, have formulated the theory of torsion of composite materials with the cylindrical geometry of circular sections and idealized the system following *de Saint-Venant's* [1856] hypothesis (i.e., each section rotates as a rigid body without any distortion and is free to warp along the torsion axis, but the warping is the same for all sections for a given constant rate of twist). Later studies [e.g., *Deimel*, 1935; *Mises*, 1945; *Packham and Sahil*, 1978] showed that during Saint-Venant torsion, any plane orthogonal to the cylinder axis does not deform on the same plane (i.e., the velocity gradients acting on the plane are zero, Figure 6c). *Feng et al.* [1996] experimentally described that the motion of solid particles (spherical and rod-like) suspended within a viscoelastic fluid only migrate radially along the shear flow direction under the action of normal stress. However, it has been also argued that if the fluid has strong normal stresses and the deformation rate is sufficiently high, the fluid may segregate from solid particles and concentrate along the outer rim of the sample [*Bartram et al.*, 1975]. In our experiments, as the twist rate was low and no textural observation supports the contention, we rule out the possibility of migration of crystals and melt orthogonal to the rotation axis.

[16] The rock deformation experiments and the results reported in this work provide a first-order estimate on the melt generation and crystallization in a metapelitic system with specific composition at constant confining pressure and temperature. The data will vary with different compositions and other experimental conditions. The range of finite shear strain is large enough ($\gamma_{\max} = 1\text{--}15$) to be comparable with natural rocks. On the other hand, the strain rate is in narrow range ($\dot{\gamma}_{\max} = 10^{-5}\text{--}10^{-4} \text{ s}^{-1}$), which is a well-identified problem in up-scaling laboratory deformation experiments to natural conditions. Because of experimental constraints, we also could not produce data for high finite strain at relatively lower strain rate, as long-term experiments are not feasible in the gas apparatus.

5. Conclusion

[17] A series of laboratory deformation experiments on synthetic quartz-muscovite aggregates at elevated confining pressure and temperature documents the dependence of deformation induced partial melting and crystallization on strain and strain rate. The results indicate that strain rate and the magnitude of strain at isothermal and isobaric conditions greatly influences the kinetics of partial melting and crystallization of a melting rock. Crystallization becomes dominant with increasing strain rate. In contrast, at constant strain rate, partial melting dominates up to moderate strain ($\gamma_{\max} < 7$). This process reverses at higher strain and the rocks contain more new crystals than melt. Application of the experimental data to geological system implies that a significant amount (~21%) of melt can be generated at high strain rate and moderate strain ($\gamma \sim 5\text{--}7$) in metapelites, but the system becomes melt-depleted at higher finite strain. At low strain rates and strain the system can contain more than 25% partial melt. Since melt-rich migmatites are low-viscosity rocks, they focus shear deformation and cause

levels of crustal decoupling. Under high strain rate and strain, decoupling should take place in a brittle-ductile mode. This is consistent with the many coexisting foliations and crosscutting vein sets commonly described in migmatites.

[18] **Acknowledgments.** Robert Hoffman and Karsten Kunze (EMEZ, ETH) are acknowledged for their assistance with technical support and electron microscopy, respectively. We sincerely acknowledge the contribution of the late Luigi Burlini to this project. Thanks to Sumit Chakraborty, James Connolly, and Elizaveta Tumarkina for useful comments and discussion with the authors during the preparation of the manuscript. This work is a part of Swiss National Fond project (200021-116153).

References

- Ashworth, J. R. (1985), *Migmatites*, 302 pp., Blackie, Glasgow, U. K.
- Barborza, S. A., and G. W. Bergantz (1998), Rheological transition and the progress of melting of crustal rocks, *Earth Planet. Sci. Lett.*, *158*, 19–29, doi:10.1016/S0012-821X(98)00047-8.
- Bartram, E., L. Goldsmith, and G. Masons (1975), Particle motion in non-Newtonian media III. Further observations in elasticoviscous fluids, *Rheol. Acta*, *14*, 776–782, doi:10.1007/BF01521406.
- Béjina, F., O. Jaoul, and R. C. Liebermann (2003), Diffusion in minerals at high pressure: A review, *Phys. Earth Planet. Inter.*, *139*, 3–20, doi:10.1016/S0031-9201(03)00140-7.
- Block, L., and L. H. Royden (1990), Core complex geometries and regional scale flow in the lower crust, *Tectonics*, *9*, 557–567, doi:10.1029/TC009i004p00557.
- Brady, J. B. (1995), Diffusion data for silicate minerals, glasses, and liquids, in *Mineral Physics and Crystallography: A Handbook of Physical Constants*, *AGU Ref. Shelf*, vol. 2 edited by T. J. Ahrens, pp. 269–290, AGU, Washington, D. C.
- Brearley, A. J., and D. C. Rubie (1990), Effects of H₂O on the disequilibrium breakdown of muscovite + quartz, *J. Petrol.*, *31*, 925–956.
- Brown, M. (2001), Orogeny, migmatites and leucogranites: A review, *Proc. Indian Acad. Sci. Earth Planet. Sci.*, *110*, 313–336.
- Burg, J.-P., and J. L. Vigneresse (2002), Non-linear feedback loops in the rheology of cooling-crystallizing felsic magma and heating-melting felsic rock, in *Deformation Mechanisms, Rheology and Tectonics: Current and Future Perspectives*, edited by S. De Meer et al., *Geol. Soc. Spec. Publ.*, *200*, 275–292.
- Deimel, R. F. (1935), The torsion of a circular cylinder, *Proc. Natl. Acad. Sci. U. S. A.*, *21*, 637–642, doi:10.1073/pnas.21.12.637.
- Dell'Angelo, L. N., and J. Tullis (1988), Experimental deformation of partially melted granitic aggregates, *J. Metamorph. Geol.*, *6*, 495–515, doi:10.1111/j.1525-1314.1988.tb00436.x.
- de Saint-Venant, A. J.-C. B. (1856), Mémoire sur la Torsion des Prismes, *Mem. Acad. Sci. Inst. Fr.*, *14*, 233–560.
- Dingwell, D. B. (1997), The brittle-ductile transition in high-level granitic magmas: Material constraints, *J. Petrol.*, *38*, 1635–1644, doi:10.1093/ptrology/38.12.1635.
- Feng, J., Y. Huang, and D. D. Joseph (1996), Dynamic simulations of sedimentation of solid particles in an Oldroyd-B fluid, *J. Non-Newtonian Fluid Mech.*, *63*, 63–88, doi:10.1016/0377-0257(95)01412-8.
- Hamilton, W. B. (2007), Earth's first two billion years—The era of internally mobile crust, *Mem. Geol. Soc. Am.*, *200*, 233–296, doi:10.1130/2007.1200(13).
- Holtzman, B. K., N. J. Groebner, M. E. Zimmerman, S. B. Ginsberg, and D. L. Kohlstedt (2003), Stress-driven melt segregation in partially molten rocks, *Geochem. Geophys. Geosyst.*, *4*(5), 8607, doi:10.1029/2001GC000258.
- Holyoke, C. W., III, and T. Rushmer (2002), An experimental on grain scale melt segregation mechanisms in two common crustal rock types, *J. Metamorph. Geol.*, *20*, 493–512, doi:10.1046/j.1525-1314.2002.00381.x.
- Janeschitz-Kriegl, H., E. Ratajski, and M. Stadlbauer (2003), Flow as an effective promoter of nucleation in polymer melts: A quantitative evaluation, *Rheol. Acta*, *42*, 355–364, doi:10.1007/s00397-002-0247-x.
- Jordan, P. J. (1987), The deformation behaviour of biminerale limestone-halite aggregates, *Tectonophysics*, *135*, 185–197, doi:10.1016/0040-1951(87)90160-0.
- Keller, A., and H. W. H. Kolnaar (1998), Flow-induced orientation and structure formation, in *Material Science and Technology*, vol. 18, *Processing of Polymers*, edited by H. E. H. Meijer, Chapter 4, Wiley-VCH, Weinheim, Germany.

- King, D. S. H., M. E. Zimmerman, and D. L. Kohlstedt (2010), Stress-driven melt segregation in partially molten olivine-rich rocks deformed in torsion, *J. Petrol.*, *51*, 21–42, doi:10.1093/ptrology/egp062.
- Kirby, S. H., and A. K. Kronenberg (1987), Rheology of the lithosphere: Selected topics, *Rev. Geophys.*, *25*, 1219–1244, doi:10.1029/RG025i006p01219.
- Lagasse, R. R., and B. Maxwell (1976), An experimental study of the kinetics of polymer crystallization during shear flow, *Polym. Eng. Sci.*, *16*, 189–199, doi:10.1002/pen.760160312.
- Laporte, D., and E. B. Watson (1995), Experimental and theoretical constraints on melt distribution in crustal sources: The effect of crystalline anisotropy on melt interconnectivity, *Chem. Geol.*, *124*, 161–184, doi:10.1016/0009-2541(95)00052-N.
- Mehnert, K. R. (1968), *Migmatites and the Origin of Granitic Rocks*, 393 pp., Elsevier, Amsterdam.
- Mises, R. V. (1945), On Saint-Venant's principle, *Bull. Am. Math. Soc.*, *51*, 555–563, doi:10.1090/S0002-9904-1945-08394-3.
- Misra, S., L. Burlini, and J.-P. Burg (2009), Strain localization and melt-segregation in deforming metapelites, *Phys. Earth Planet. Inter.*, *177*, 173–179, doi:10.1016/j.pepi.2009.08.011.
- Packham, B. A., and R. Sahil (1978), St. Venant torsion of composite cylinders, *J. Elast.*, *8*, 393–407, doi:10.1007/BF00049189.
- Paterson, M. S., and D. L. Olgaard (2000), Rock deformation tests to large shear strains in torsion, *J. Struct. Geol.*, *22*, 1341–1358, doi:10.1016/S0191-8141(00)00042-0.
- Ramsay, J. G. (1980), Shear zone geometry: A review, *J. Struct. Geol.*, *2*, 83–99, doi:10.1016/0191-8141(80)90038-3.
- Renner, J., B. Evans, and G. Hirth (2000), On the rheologically critical melt fraction, *Earth Planet. Sci. Lett.*, *181*, 585–594, doi:10.1016/S0012-821X(00)00222-3.
- Rosenberg, C. L., and M. R. Handy (2000), Syntectonic melt pathways during simple shearing of a partially molten rock analogue (Norcamphor-Benzamide), *J. Geophys. Res.*, *105*(B2), 3135–3149, doi:10.1029/1999JB900371.
- Rushmer, T. (1995), An experimental deformation study of partially molten amphibolite: Application to low-melt fraction segregation, *J. Geophys. Res.*, *100*(B8), 15,681–15,695, doi:10.1029/95JB00077.
- Rutter, E. H., and D. H. K. Neumann (1995), Experimental deformation of partially molten Westerly granite under fluid-absent conditions, with implications for the extraction of granitic magmas, *J. Geophys. Res.*, *100*(B8), 15,697–15,715, doi:10.1029/94JB03388.
- Tanner, R. I., and F. Qi (2005), A comparison of some models for describing polymer crystallization at low deformation rates, *J. Non-Newtonian Fluid Mech.*, *127*, 131–141, doi:10.1016/j.jnnfm.2005.02.005.
- Vanderhaeghe, O., and C. Teyssier (2001), Partial melting and flow of orogens, *Tectonophysics*, *342*, 451–472, doi:10.1016/S0040-1951(01)00175-5.
- Vanderhaeghe, O., J.-P. Burg, and C. Teyssier (1999), Exhumation of migmatites in two collapsed orogens: Canadian Cordillera and French Variscides, in *Collisional Belts and Intra-Continental Convergence (A-Type Subduction)*, edited by U. Ring et al., *Geol. Soc. Spec. Publ.*, *154*, 181–204.
- van der Molen, I., and M. S. Paterson (1979), Experimental deformation of partially melted granite, *Contrib. Mineral. Petrol.*, *70*, 299–318, doi:10.1007/BF00375359.
- Vigneresse, J. L., and J.-P. Burg (2004), Strain-rate-dependent rheology of partially molten rocks, in *Vertical Coupling and Decoupling in the Lithosphere*, edited by J. Grocott et al., *Geol. Soc. Spec. Publ.*, *227*, 327–336.
- Vigneresse, J. L., and B. Tikoff (1999), Strain partitioning during partial melting and crystallization with application to felsic magma and transfer, *Tectonophysics*, *312*, 117–132, doi:10.1016/S0040-1951(99)00167-5.
- Vigneresse, J. L., P. Barbey, and M. Cuney (1996), Rheological transitions during partial melting and crystallization with application to felsic magma segregation and transfer, *J. Petrol.*, *37*, 1579–1600, doi:10.1093/ptrology/37.6.1579.
- Watson, E. B., and E. F. Baxter (2007), Diffusion in solid-Earth systems, *Earth Planet. Sci. Lett.*, *253*, 307–327, doi:10.1016/j.epsl.2006.11.015.
- Zheng, R., and P. K. Kennedy (2004), A model for post-flow induced crystallization: General equations and predictions, *J. Rheol. N. Y.*, *48*, 823–842, doi:10.1122/1.1763944.
- Zimmerman, M. E., S. Zhang, D. L. Kohlstedt, and S. Karato (1999), Melt distribution in mantle rocks deformed in shear, *Geophys. Res. Lett.*, *26*, 1505–1508, doi:10.1029/1999GL900259.

J.-P. Burg and S. Misra, Structural Geology and Tectonics Group, Geological Institute, ETH, Sonneggstrasse 05, CH-8092 Zurich, Switzerland. (santanu.misra@erdw.ethz.ch)

D. Mainprice, Géosciences Montpellier UMR CNRS 5243, Université Montpellier 2, F-34095 Montpellier CEDEX 05, France.